ACCSCIENCE PUBLISHING

Materials Science in Additive Manufacturing

SHORT COMMUNICATION

Effect of lattice interlocking geometry on curing distribution and tensile performance in metal–polymer hybrid structures fabricated by powder bed fusion and vat photopolymerization

Min-Seong Ko[1,2] and Do-Sik Shim[1,2]*

[1]Department of Ocean Advanced Materials Convergence Engineering, College of Engineering, Korea Maritime and Ocean University, Busan, Republic of Korea

[2]Department of Interdisciplinary Major of Ocean Renewable Energy Engineering, College of Graduate School, Korea Maritime and Ocean University, Busan, Republic of Korea

***Corresponding author:**
Do-Sik Shim
(think@kmou.ac.kr)

Citation: Ko MS, Shim DS. Effect of lattice interlocking geometry on curing distribution and tensile performance in metal–polymer hybrid structures fabricated by powder bed fusion and vat photopolymerization. *Mater Sci Add Manuf.* 2026;5(3):026190039. doi: 10.36922/MSAM026190039

Received: May 4, 2026

Revised: June 12, 2026

Accepted: June 22, 2026

Published online: July 15, 2026

Abstract

Metal–polymer hybrid structures can be fabricated by integrating powder bed fusion (PBF) and vat photopolymerization (VPP) additive manufacturing, in which a photopolymer is infiltrated and cured within metal lattice structures through extended UV exposure. This study examines how the lattice interlocking geometry influences local curing behavior and the tensile performance of hybrid structures. Four lattice geometries, simple cubic (SC), face-centered cubic (FCC), body-centered cubic (BCC), and pyramid, were comparatively investigated. Indirect curing enabled polymer solidification within optically shielded lattice regions, but the curing level decreased with increasing distance from the incident surface, resulting in geometry-dependent microhardness distributions. Tensile behavior also depended strongly on lattice geometry: FCC and BCC showed the highest maximum loads of 1,115 and 1,111 N, respectively, whereas SC and pyramid exhibited lower values of 834 and 742 N, respectively. Fracture observations indicated that FCC and BCC promoted more tortuous crack paths through inclined or diagonal struts, while SC and pyramid provided less favorable fracture routes and lower resistance. These results show that lattice geometry governs the tensile performance of PBF–VPP metal–polymer hybrid structures by influencing both curing distribution and fracture path.

Keywords: Vat photopolymerization; Powder bed fusion; Metal–polymer hybrid structures; Mechanical interlocking; Tensile behavior

1. Introduction

Metal–polymer hybrid structures have attracted increasing attention because they can combine the high strength and stiffness of metals with the low density, processing flexibility, and functional versatility of polymers. In such systems, interfacial design is a key factor, as the large mismatch in mechanical and thermal properties of metals and polymers often limits load transfer and structural reliability. Mechanical interlocking has therefore been regarded as an effective strategy for improving metal–polymer joining performance, since the interfacial geometry can directly influence polymer infiltration, local stress transfer, and crack propagation.[1-10] However, conventional joining methods have limited capability to fabricate complex three-dimensional interlocking architectures with well-controlled internal geometry.

Additive manufacturing offers a promising route to overcome this limitation by enabling the direct fabrication of complex metallic interlocking structures that are difficult to realize by conventional machining or joining methods. Previous studies have demonstrated hybrid metal–polymer fabrication through combinations of metal and polymer additive manufacturing processes and have shown that interlocking geometry can strongly affect joining performance.[11-15] Among polymer additive manufacturing techniques, vat photopolymerization (VPP) is particularly attractive because of its high dimensional resolution and suitability for fabricating fine structural features.[16-18] In addition, prolonged light exposure in VPP can induce indirect curing in partially shielded regions through light transmission and scattering.[19,20] Although this over-curing behavior is often considered a source of dimensional inaccuracy, it can also be utilized to infiltrate and solidify polymer within internal metallic structures.

Based on these characteristics, this study proposes an integrated manufacturing approach in which a metal lattice is first fabricated by powder bed fusion (PBF), followed by polymer filling through the over-curing behavior of VPP. This approach enables integrated metal–polymer hybrid structures to be fabricated within a single additive manufacturing workflow. Owing to the high resolution of VPP and the structural reinforcement provided by metallic lattices, such structures have potential for lightweight, high-precision engineering components with complex geometries in aerospace, automotive, and marine applications. The aim of this study is to clarify how lattice geometry affects indirect curing distribution, tensile performance, and fracture path in integrated PBF–VPP hybrid structures, and to identify the geometric features favorable for mechanically interlocked metal–polymer interfaces.

2. Methods

Metal–polymer hybrid structures were fabricated through a sequential combination of PBF and VPP additive manufacturing processes. The overall fabrication concept and the investigated lattice geometries are shown in Figure 1. Figure 1a schematically illustrates the over-curing-based filling process employed in this study. The three VPP curing stages represent the progressive expansion of the cured polymer region within the metallic lattice under extended UV exposure. Three-dimensional models were designed using CATIA V5 (Dassault Systèmes, France) and converted into STL files. Metal lattice structures were fabricated from SUS630 (17-4PH) stainless steel powder using an SLM 280 V2.0 system (SLM Solutions, Germany). The main PBF parameters were a laser power of 200 W, a scanning speed of 800 mm/s, a hatch distance of 120 µm, and a layer thickness of 30–60 µm. The powder particle size ranged from 10 to 45 µm.

The polymer component was fabricated using a bottom-up, masked stereolithography-based VPP system (Phenom Forge, Peopoly Inc., Hong Kong) equipped with a 405 nm UV light-emitting diode (LED). A commercially available photocurable resin, Resione M58 (Dongguan Godsaid Technology Co., Ltd., China), was used. The normal layer thickness and exposure time were 50 µm and 2.5 s. To induce polymer infiltration into the internal lattice region, the PBF-fabricated metal structures were immersed in the liquid resin and exposed to UV light for an extended duration. This prolonged exposure promoted indirect curing in optically shielded regions through transmitted and scattered light, enabling resin solidification within the metal lattices. After the infiltration step, the VPP process was continued to complete the polymer region of the hybrid tensile specimen.

The simple cubic (SC), face-centered cubic (FCC), body-centered cubic (BCC), and pyramid lattices investigated in this study were designed to possess the same relative densities by adjusting the strut diameter of each geometry, thereby enabling a fair comparison of geometry-dependent effects, as shown in Figure 1b. The unit-cell size was fixed at 1 mm for all cases. Hybrid tensile specimens were designed on the basis of ASTM D638 Type I geometry with reduced overall dimensions, and the metal interlocking region consisted of a 6 × 6 array of unit cells, resulting in a square area of 6 × 6 mm^2. The fabricated hybrid specimens and representative cross-sectional observations are shown in Figure 2. In the study, cross-sectional images were observed using an optical microscope (OM; VHX-7000, KOREA KEYENCE Co., Ltd., Korea). Tensile tests were conducted using a universal testing machine at a crosshead speed of 2 mm/s, and microhardness measurements were carried out to evaluate the depth-wise curing distribution of the infiltrated polymer within the metal lattices.

3. Results and discussion

3.1. Fabrication of hybrid structures

The integrated fabrication process successfully produced hybrid metal–polymer tensile specimens for all investigated lattice geometries. As shown in Figure 2a, the metal holder, PBF-fabricated lattice, and VPP-printed polymer region were integrated into a single specimen. Cross-sectional observations in Figure 2b confirmed that

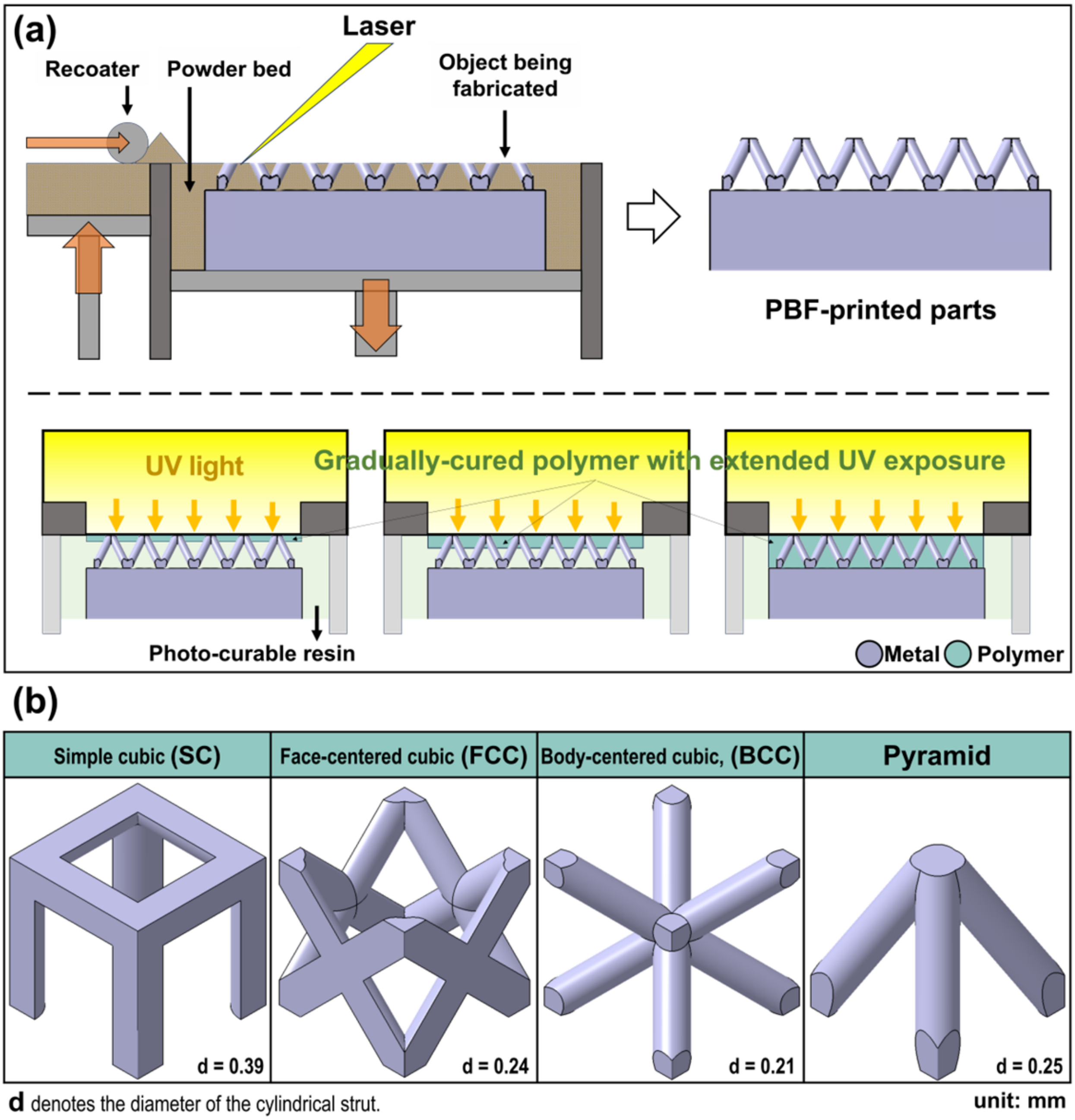

Figure 1. Schematic illustration of the integrated powder bed fusion (PBF)–vat photopolymerization (VPP) process and investigated lattice interlocking geometries. (a) Fabrication concept of the metal–polymer hybrid structure, in which a metal lattice was first produced by PBF, followed by photopolymer infiltration and indirect curing through extended UV exposure during VPP. (b) Unit-cell geometries investigated in this study: simple cubic (SC), face-centered cubic (FCC), body-centered cubic (BCC), and pyramid.

the photopolymer filled the internal spaces of the metal lattices in all cases, indicating that the selected over-curing condition was sufficient to form the interlocking hybrid structure. These results demonstrate that indirect curing during VPP, primarily driven by light scattering within the photopolymer, can be utilized to fabricate mechanically interlocked hybrid interfaces within PBF-produced metal lattices.[21-24]

3.2. Geometry-dependent curing distribution

The curing state within the interlocking region was strongly dependent on lattice geometry. As shown in Figure 3, the

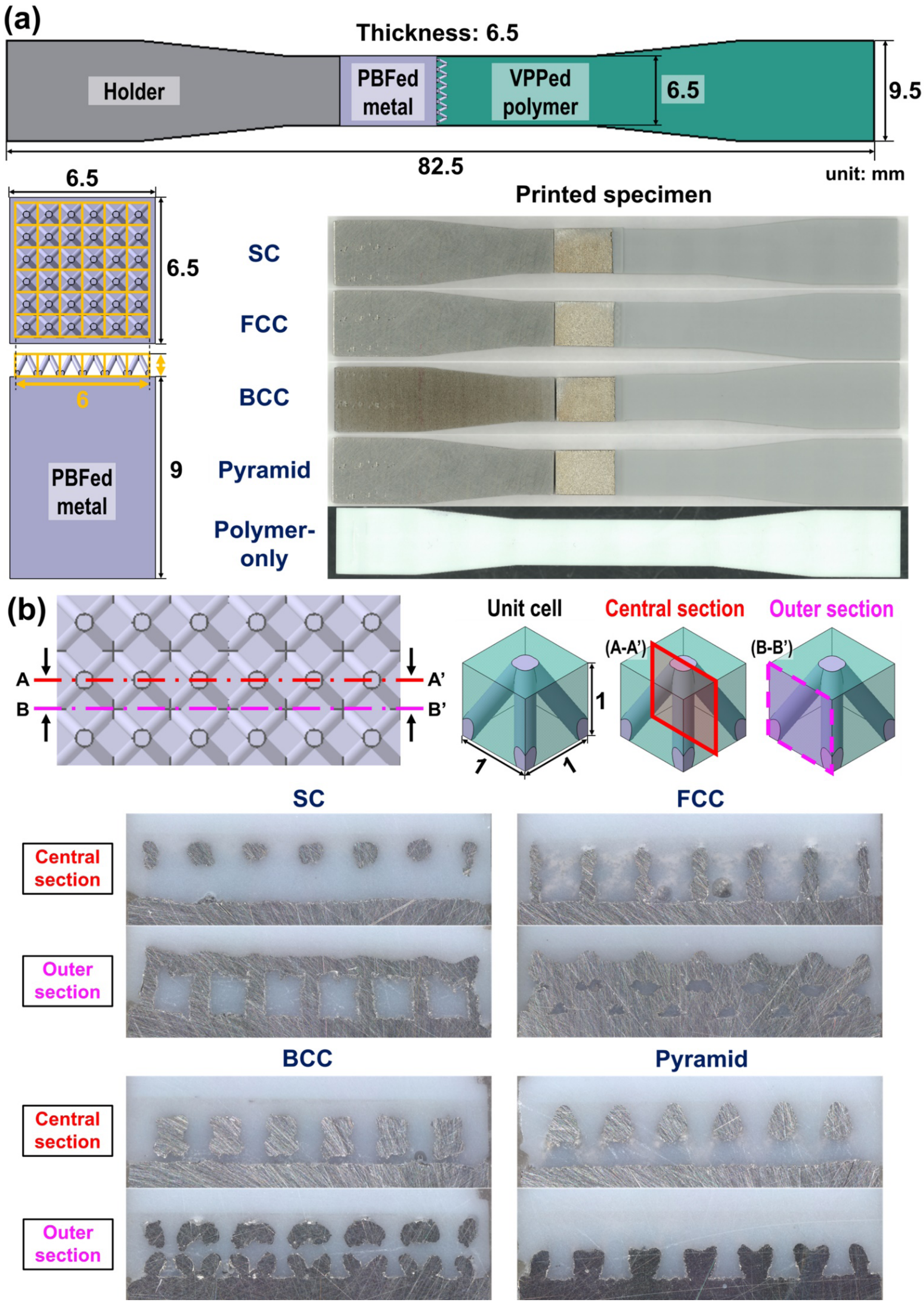

Figure 2. Fabricated hybrid tensile specimens and representative cross-sectional observations of the interlocking region. (a) Overall views of the metal–polymer hybrid tensile specimens fabricated by the integrated powder bed fusion (PBF)–vat photopolymerization (VPP) process. (b) Cross-sectional images of the interlocking region, showing polymer filling and curing within the internal spaces of the PBF-fabricated metal lattices for all investigated geometries.

Abbreviations: BCC: Body-centered cubic; FCC: Face-centered cubic; SC: Simple cubic.

depth-wise microhardness of the infiltrated photopolymer decreased with increasing distance from the incident surface in all geometries. Because the mechanical response of photocurable resins is closely related to the local extent of polymerization, the measured hardness gradient can be interpreted as evidence of a non-uniform curing state within the lattice. This tendency indicates that the effective optical energy delivered into the interlocking region decreased with depth due to the progressive attenuation of incident light within the metallic structure. Although microhardness does not directly quantify the degree of conversion or interfacial bonding state, it is widely used as a practical indicator of curing behavior in photocurable resins because it reflects the evolution of polymer network formation driven by over-curing and the resulting increase in degree of conversion. Therefore, the measured hardness distribution was used in this study as a practical indicator of the spatial variation in curing effectiveness within the lattice.[25-29]

The hardness distributions further showed that the curing behavior was not governed solely by the exposure condition, but also by the three-dimensional topology of the lattice. Although all specimens were processed under identical irradiation conditions, the SC, FCC, BCC, and pyramid geometries exhibited different depth-wise hardness profiles. This result indicates that the internal arrangement of the metallic struts modified the local optical shielding condition and, consequently, the spatial distribution of curing within the polymer-filled region. Therefore, the effective curing state was controlled not only by the nominal exposure parameters, but also by the geometry-dependent light paths available within each lattice.

This geometry-dependent curing distribution is mechanically important because tensile load was transferred through a polymer phase constrained within the metallic interlocking structure. Under such conditions, non-uniform curing is expected to generate spatial variations in local stiffness and fracture resistance within the polymer-filled region. Therefore, the mechanical performance of the present hybrid structures should be interpreted not only in terms of whether polymer infiltration was achieved, but also in terms of how uniformly a mechanically effective polymer phase was established within the lattice. From this perspective, the curing gradient shown in Figure 3 provides a mechanistic basis for understanding the geometry-dependent tensile and fracture behavior discussed in the following sections.

3.3. Geometry-dependent tensile behavior

The tensile response of the hybrid structures showed a pronounced dependence on lattice geometry, as presented

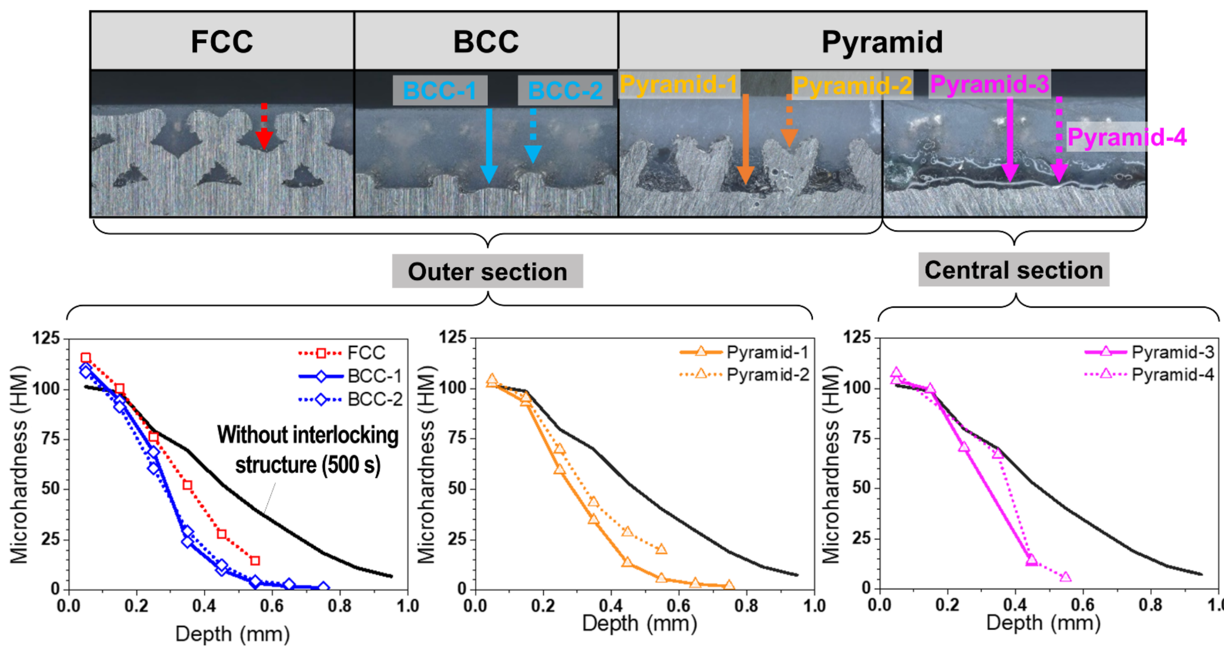

Figure 3. Geometry-dependent microhardness distributions of the infiltrated photopolymer within the metal lattices. The depth-wise hardness profiles show that the local curing state decreased with increasing distance from the incident surface and varied depending on lattice geometry, indicating non-uniform curing behavior within the interlocking region.
Abbreviations: BCC: Body-centered cubic; FCC: Face-centered cubic.

in Figure 4a and 4b. FCC and BCC exhibited the highest maximum loads, 1,115 and 1,111 N, respectively, whereas SC and pyramid showed lower values of 834 and 742 N, respectively. In addition, FCC and BCC sustained tensile loads comparable to those of the polymer reference specimens with the corresponding geometries, while SC and pyramid showed a more substantial reduction in load-carrying capacity. FCC and BCC achieved maximum loads comparable to those of the polymer-only specimen while sustaining large tensile displacements through effective load transfer within the metallic interlocking structure. The polymer-only specimen exhibited continuous deformation associated with the intrinsic viscoelastic behavior of the cured resin. These results indicate that the tensile performance of the hybrid structures was governed not simply by polymer filling, but also by the extent to which the lattice geometry enabled efficient load transfer and resisted crack propagation within the interlocking region.

The geometric indicators summarized in Figure 4c help to interpret this tendency, although they do not directly determine tensile performance. The investigated lattices were designed to have comparable polymer-filled volume fractions (ρ = 79.8–80.6%), whereas the indirectly cured area fractions (ρ = 15.6–43.1%) and the projected metal

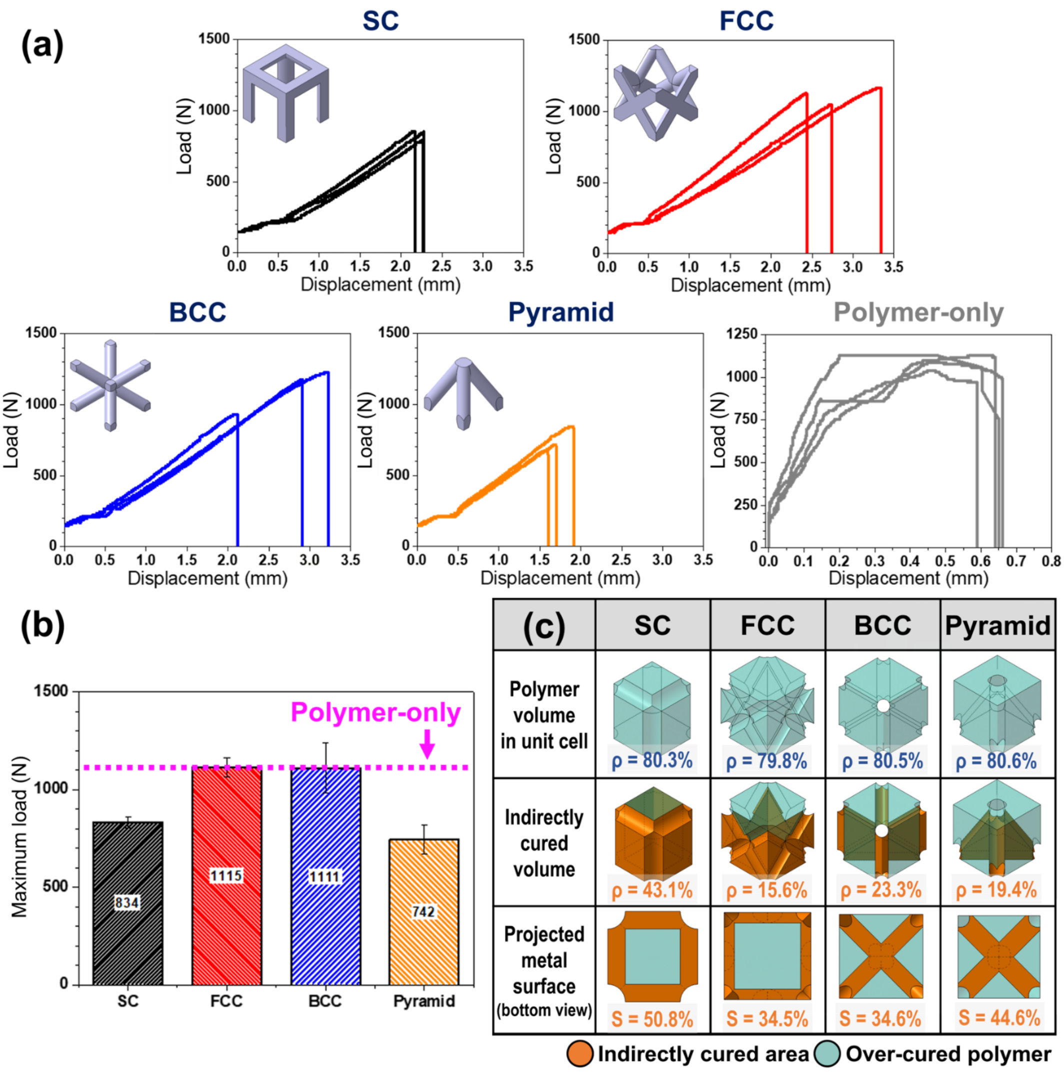

Figure 4. Geometry-dependent tensile behavior of the hybrid structures. (a) Load–displacement curves of the hybrid specimens and polymer-only specimens with the corresponding lattice geometries. (b) Comparison of the maximum tensile loads for simple cubic (SC), face-centered cubic (FCC), body-centered cubic (BCC), and pyramid. (c) Geometric indicators of the lattice structures, including the volume fraction of the indirectly cured region and the projected metal surface fraction at the incident surface.

surface fractions (S = 34.5–50.8%) varied significantly depending on the lattice geometry. This result suggests that no single geometric metric alone is sufficient to explain the observed tensile behavior. Instead, the load-carrying capacity was governed by the combined effects of local curing effectiveness and geometry-dependent crack-path control. Accordingly, the load-carrying capacity was enhanced when the lattice architecture provided effective load-transfer paths and resistance to crack propagation through the interlocking region.

From this perspective, the superior performance of FCC and BCC can be attributed to their inclined or diagonal strut networks, which provided greater resistance to direct crack propagation during tensile loading. The lower maximum loads observed for SC and pyramid indicate that tensile resistance was strongly influenced by crack-path control and load-transfer efficiency. These results demonstrate that the tensile behavior of the present hybrid structures was governed by the combined effects of local curing effectiveness and lattice topology.

3.4. Fracture behavior of the hybrid interface

Fractographic observations revealed that the failure behavior of the hybrid specimens was strongly governed by lattice geometry. Fracture characteristics were identified directly from the exposed metal lattice on the fracture surface, supported by cross-sectional OM of sectioned specimens. As shown in Figure 5a, the fracture did not propagate along a single planar interface in any of the investigated specimens. Instead, the crack path was constrained by the three-dimensional topology of the metallic interlocking structure, resulting in distinct

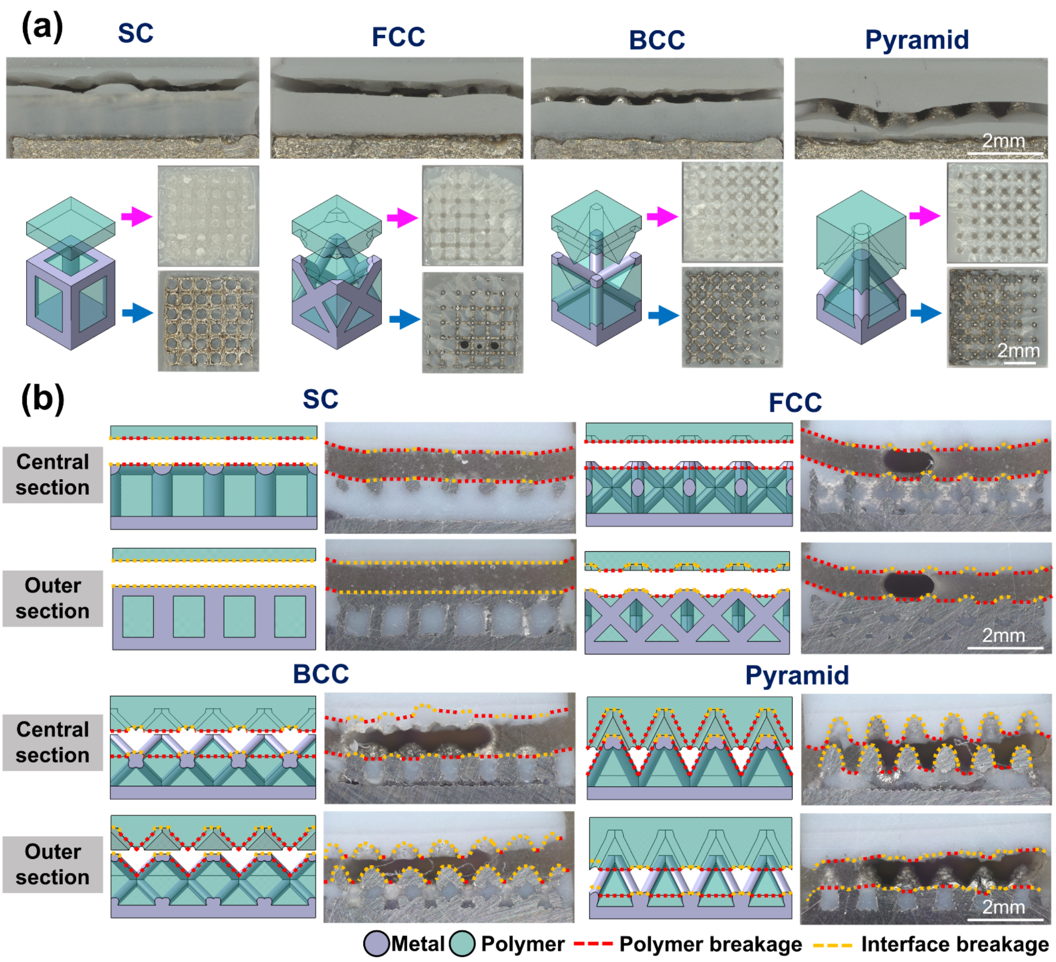

Figure 5. Geometry-dependent fracture behavior of the hybrid interfaces after tensile testing. (a) Representative side and top views of the fractured hybrid specimens, showing that the fracture morphology varied with lattice geometry. (b) Cross-sectional observations of the fracture paths in the interlocking region, indicating that face-centered cubic (FCC) and body-centered cubic (BCC) promoted more tortuous crack propagation, whereas simple cubic (SC) and pyramid provided less favorable fracture routes. Scale bars: 2 mm; magnifications: 50×.

fracture morphologies for SC, FCC, BCC, and pyramid. These results demonstrate that the tensile performance of the present hybrid structures is governed by geometry-controlled crack propagation within the interlocking region.

The cross-sectional fracture paths shown in Figure 5b further clarify the origin of the geometry-dependent tensile response. In the FCC and BCC structures, crack propagation was repeatedly deflected by inclined or diagonal struts, leading to a more tortuous fracture path through the interlocking region. Such a crack path is expected to increase the effective propagation length and to suppress direct interfacial separation under tensile loading. This geometry-induced crack deflection is considered the primary reason why FCC and BCC exhibit higher load-carrying capacity than SC and pyramid. The present tendency is consistent with previous studies showing that structured interfaces can improve mechanical resistance by increasing crack-path complexity and delaying unstable separation.[30-32]

By contrast, the SC and pyramid geometries exhibited lower resistance to crack propagation, although the underlying reasons differed. In the SC structure, the predominance of vertical struts provided a relatively direct fracture path once local damage was initiated, thereby limiting the extent of crack deflection within the interlocking region. This structural characteristic is considered to have reduced resistance to crack propagation and contributed to the lower tensile performance of SC. In the pyramid structure, fracture propagated preferentially along the inclined lattice surfaces and developed in a region located farther from the incident surface. As discussed in Section 3.2, the deeper region of the lattice showed a lower local curing state, as inferred from the reduced microhardness. Therefore, the inferior tensile performance of the pyramid specimen is attributed not only to its comparatively direct propagation path, but also to fracture development within a mechanically less effective polymer region.

Overall, these results demonstrate that the fracture resistance of the present hybrid interfaces was governed by the combined effects of lattice topology and local curing distribution. In particular, the results highlight that an effective interlocking geometry should not only ensure polymer infiltration but also promote crack-path deflection and prevent fracture from localizing in insufficiently cured regions of the interlocking structure.

4. Conclusion

This study demonstrated that integrated PBF–VPP additive manufacturing can produce mechanically interlocked metal–polymer hybrid structures by curing photopolymer within PBF-fabricated metal lattices through extended UV exposure. Lattice geometry strongly affected the local curing distribution, tensile load-carrying capacity, and fracture path of the hybrid structures. FCC and BCC structures exhibited superior tensile properties due to their inclined and diagonal strut architectures, which promote crack deflection and distributed load transfer. In contrast, SC structures facilitated more direct fracture paths, while pyramid structures experienced fracture initiation in deeper, less effectively cured regions, leading to reduced performance. These results indicate that the key geometric feature governing mechanical performance is the ability to control crack-path tortuosity while maintaining fracture within sufficiently cured regions. In particular, inclined and diagonally connected strut networks are identified as beneficial design features for enhancing fracture resistance in hybrid lattices. Overall, the tensile behavior is governed primarily by lattice geometry, while polymer curing heterogeneity plays a secondary role in modulating local fracture behavior.

Acknowledgments

None.

Funding

This work was supported by the Korea Research Institute for Defense Technology Planning and Advancement (KRIT) grant funded by the Defense Acquisition Program Administration (DAPA) (KRIT-CT-23-007) and the Korea Basic Science Institute (National Research Facilities and Equipment Center) grant funded by the Ministry of Education (grant No. 2022R1A6C101B738). Additional support from the National Research Foundation of Korea (NRF) under grant number RS-2024-00346166602820634901O1, funded by the Ministry of Science and ICT, is gratefully acknowledged.

Conflict of interest

The authors declare no conflict of interest.

Author contributions

Conceptualization: Do-Sik Shim
Data curation: Min-Seong Ko
Investigation: Min-Seong Ko
Methodology: Min-Seong Ko
Supervision: Do-Sik Shim
Writing–original draft: Min-Seong Ko
Writing–review & editing: Min-Seong Ko, Do-Sik Shim

Ethics approval and consent to participate

Not applicable.

Consent for publication

Not applicable.

Availability of data

The data are available from the corresponding author upon reasonable request.

References

1. Delzendehrooy F, Akhavan-Safar A, Barbosa AQ, *et al*. A comprehensive review on structural joining techniques in the marine industry. *Compos Struct*. 2022;289.

doi: 10.1016/j.compstruct.2022.115490

2. Huang Y, Gao X, Zhang Y, Ma B. Laser joining technology of polymer-metal hybrid structures - A review. *J Manuf Process*. 2022;79:934-961.

doi: 10.1016/j.jmapro.2022.05.026

3. Lambiase F, Scipioni SI, Lee CJ, Ko DC, Liu F. A state-of-the-art review on advanced joining processes for metal-composite and metal-polymer hybrid structures. *Materials*. 2021;14(8).

doi: 10.3390/ma14081890

4. Lambiase F, Liu F. Recent advances in metal-polymer joining processes. In: *Joining Processes for Dissimilar and Advanced Materials*. Amsterdam, Netherlands: Elsevier; 2022:123-151.

doi: 10.1016/B978-0-323-85399-6.00007-2

5. Borges CSP, Akhavan-Safar A, Tsokanas P, Carbas RJC, Marques EAS, da Silva LFM. From fundamental concepts to recent developments in the adhesive bonding technology: a general view. *Discov Mech Eng*. 2023;2(1).

doi: 10.1007/s44245-023-00014-7

6. Wei Y, Jin X, Luo Q, Li Q, Sun G. Adhesively bonded joints – A review on design, manufacturing, experiments, modeling and challenges. *Compos Part B Eng*. 2024;276.

doi: 10.1016/j.compositesb.2024.111225

7. Bu H, Li X, Wang J, Li B, Xiao L, Zhan X. Porosity characteristics and interfacial structure evolution of laser joining CFRTP and 6061-T6 with prefabricated interfacial grooves. *Compos Part B Eng*. 2025;294.

doi: 10.1016/j.compositesb.2025.112173

8. Du M, Dong W, Li X, Wang L, Wang B, Tang B. Effect of surface topography on injection joining Ti alloy for improved bonding strength of metal-polymer. *Surf Coat Technol*. 2022;433.

doi: 10.1016/j.surfcoat.2022.128132

9. Vasconcelos RL, Oliveira GHM, Amancio-Filho ST, Canto LB. Injection overmolding of polymer-metal hybrid structures: A review. *Polym Eng Sci*. 2023;63(3):691-722.

doi: 10.1002/pen.26244

10. Kimura F, Kadoya S, Kajihara Y. Effects of molding conditions on injection molded direct joining using a metal with nano-structured surface. *Precis Eng*. 2016;45:203-208.

doi: 10.1016/j.precisioneng.2016.02.013

11. Chueh YH, Wei C, Zhang X, Li L. Integrated laser-based powder bed fusion and fused filament fabrication for three-dimensional printing of hybrid metal/polymer objects. *Addit Manuf*. 2020;31:100928.

doi: 10.1016/j.addma.2019.100928

12. Chueh YH, Zhang X, Ke JCR, Li Q, Wei C, Li L. Additive manufacturing of hybrid metal/polymer objects via multiple-material laser powder bed fusion. *Addit Manuf*. 2020;36.

doi: 10.1016/j.addma.2020.101465

13. Abreu T, Leal RM, Leitão C, Galvão I. Metal-Polymer Joining by Additive Manufacturing: Effect of Printing Parameters and Interlocking Design. *J Manuf Mater Process*. 2024;8(5):228.

doi: 10.3390/jmmp8050228

14. Englert L, Heuer A, Engelskirchen MK, *et al*. Hybrid material additive manufacturing: interlocking interfaces for fused filament fabrication on laser powder bed fusion substrates. *Virtual Phys Prototyp*. 2022;17(3):508-527.

doi: 10.1080/17452759.2022.2048228

15. Hertle S, Kleffel T, Wörz A, Drummer D. Production of polymer-metal hybrids using extrusion-based additive manufacturing and electrochemically treated aluminum. *Addit Manuf*. 2020;33:101135.

doi: 10.1016/j.addma.2020.101135

16. Guerra Silva R, Torres MJ, Zahr Viñuela J. A comparison of miniature lattice structures produced by material extrusion and vat photopolymerization additive manufacturing. *Polymers*. 2021;13(13):2163.

doi: 10.3390/polym13132163

17. Pagac M, Hajnys J, Ma QP, *et al*. A review of vat photopolymerization technology: Materials, applications, challenges, and future trends of 3D printing. *Polymers*. 2021;13(4):598.

doi: 10.3390/polym13040598

18. Zhang F, Zhu L, Li Z, *et al*. The recent development of vat photopolymerization: A review. *Addit Manuf*. 2021;48:102423.

doi: 10.1016/j.addma.2021.102423

19. Li L, Huang Z. Vat photopolymerization 3D printing of ceramics. In: *Vat Photopolymerization Additive Manufacturing: 3D Printing Processes, Materials, and Applications*. Amsterdam, Netherlands: Elsevier; 2024:195-241.

doi: 10.1016/B978-0-443-15487-4.00007-8

20. Wang X, Liu J, Kho ASK, Hong W, Gilchrist MD, Zhang N. Elucidating the mechanism of overcuring in microchannels fabricated via vat photopolymerization (VPP) for precise microfluidic chip printing. *Addit Manuf*. 2024;92:104350.

    doi: 10.1016/j.addma.2024.104350

21. Jacobs PF. *Rapid Prototyping and Manufacturing: Fundamentals of Stereolithography*. Southfield, MI: Society of Manufacturing Engineers; 1992.

22. Li Y, Mao Q, Yin J, Wang Y, Fu J, Huang Y. Theoretical prediction and experimental validation of the digital light processing (DLP) working curve for photocurable materials. *Addit Manuf*. 2021;37:101716.

    doi: 10.1016/j.addma.2020.101716

23. Guven E, Karpat Y, Cakmakci M. Improving the dimensional accuracy of micro parts 3D printed with projection-based continuous vat photopolymerization using a model-based grayscale optimization method. *Addit Manuf*. 2022;57:102954.

    doi: 10.1016/j.addma.2022.102954

24. Qian C, Hu K, Li J, Li P, Lu Z. The effect of light scattering in stereolithography ceramic manufacturing. *J Eur Ceram Soc*. 2021;41(14):7141-7154.

    doi: 10.1016/j.jeurceramsoc.2021.07.017

25. Rehbein T, Johlitz M, Lion A, Sekmen K, Constantinescu A. Temperature- and degree of cure-dependent viscoelastic properties of photopolymer resins used in digital light processing. *Prog Addit Manuf*. 2021;6(4):743-756.

    doi: 10.1007/s40964-021-00194-2

26. Yang Y, Li L, Zhao J. Mechanical property modeling of photosensitive liquid resin in stereolithography additive manufacturing: Bridging degree of cure with tensile strength and hardness. *Mater Des*. 2019;162:418-428.

    doi: 10.1016/j.matdes.2018.12.009

27. Vallabh CKP, Zhang Y, Zhao X. In-situ ultrasonic monitoring for Vat Photopolymerization. *Addit Manuf*. 2022;55:102801.

    doi: 10.1016/j.addma.2022.102801

28. Lim JH, Shin SH, Jung YE, An H, Kim JE. Influence of heat-assisted vat photopolymerization on the physical and mechanical characteristics of dental 3D printing resins. *Sci Rep*. 2025;15(1).

    doi: 10.1038/s41598-025-85529-7

29. Zhang H, Zhang Y, Zhao X. Vat photopolymerization additive manufacturing process modeling: a thermal-chemical coupling approach informed by in-situ and ex-situ characterization data. *Addit Manuf Lett*. 2024;9:100193.

    doi: 10.1016/j.addlet.2024.100193

30. Verma S, Yang CK, Lin CH, Jeng JY. Additive manufacturing of lattice structures for high strength mechanical interlocking of metal and resin during injection molding. *Addit Manuf*. 2022;49:102463.

    doi: 10.1016/j.addma.2021.102463

31. Graziosi S, Cannazza F, Vedani M, Ratti A, Tamburrino F, Bordegoni M. Design and testing of an innovative 3D-printed metal-composite junction. *Addit Manuf*. 2020;36:101311.

    doi: 10.1016/j.addma.2020.101311

32. Lin E, Li Y, Ortiz C, Boyce MC. 3D printed, bio-inspired prototypes and analytical models for structured suture interfaces with geometrically-tuned deformation and failure behavior. *J Mech Phys Solids*. 2014;73:166-182.

    doi: 10.1016/j.jmps.2014.08.011